KARLSRUHE INSTITUTE OF TECHNOLOGY
INSTITUTE OF THEORETICAL PHYSICS (ITP)

Anomalous couplings in $t\bar{t}H$ production

Anomale Kopplungen in $t\bar{t}H$ Produktion

Bachelor's thesis

for the physics course

by

Marijn van Geest

Reviewer: Prof. Dr. Gudrun Heinrich
Second reviewer: PD Dr. Stefan Gieseke

Submitted on 16.08.2022

Declaration of Originality

I confirm that the submitted thesis is original work and was written by me without further assistance. Appropriate credit has been given where reference has been made to the work of others. I have noted the KIT Statutes for Safeguarding Good Research Practice as amended from time to time.

The thesis was not examined before, nor has it been published.

Erklärung zur Selbstständigkeit

Ich versichere, dass ich die vorliegende Arbeit selbstständig und ohne fremde Hilfe verfasst habe. Aussagen, die dem Wortlaut oder dem Sinne nach anderen Werken entommen wurden, sind durch die jeweiligen Verweise kenntlich gemacht. Ich habe die Satzung des KIT zur Sicherung guter wissenschaftlicher Praxis in der jeweils gültigen Fassung beachtet.

Diese Arbeit hat in der Vergangenheit weder an einem anderen Prüfungsverfahren teilgenommen, noch wurde sie in irgend einer Weise zuvor publiziert.

Karlsruhe, den 16.08.2022, _____

Marijn van Geest

Contents

List of Figures

List of Tables

1 Introduction

The Standard Model is one of the most important constructs in particle physics, explaining many interactions and properties of known particles. However, this model can not be fully accurate or complete, since it does not explain concepts like dark matter or the baryon asymmetry in the universe for instance. A possible explanation for the latter could be given by new sources of CP-violating properties of particles [1].

After being theoretically predicted [2–7], the Higgs boson has been discovered at around 125 GeV in 2012 at the CERN LHC Run II program [8,9], where it remained to be a focus of attention. It has been found by observing an excess in events, mainly with the $\gamma\gamma$ and ZZ decay modes [9]. Its discovery is an important step to substantiate the theory of the electroweak symmetry breaking mechanism, which is the process behind elementary particles acquiring their mass.

Besides that, this comparatively newfound particle is of great interest, due to the possibility of it having yet unknown CP-symmetry breaking properties. A selection of properties of this particle, predicted by Standard Model theory, have already been verified at the LHC, which includes its spin and parity [10]. Higgs interactions with $ZZ, Z\gamma, \gamma\gamma,$ and WW have also shown that a pure CP-odd coupling with vector bosons can be excluded with a 99.98 % confidence level [11], leaving only the possibility of a certain mixture of CP-even and CP-odd coupling components. However, the interactions with vector bosons are loop-induced, which makes them naturally suppressed. A more accessible approach is the analysis of tree-level interactions with fermions [12]. The coupling to top-quarks is particularly large, due to the mass of this quark at around 173 GeV, being the largest of the standard model. Interactions of this type are therefore a very suitable candidate for finding new physics.

A possibility to reach the Higgs-top interaction is by associated $t\bar{t}H$ production. This process has been observed independently by the CMS and ATLAS collaboration in 2018 [13, 14], therefore introducing the opportunity for using this channel in further analysis. By performing additional measurements, both collaborations also recently managed to constrain the mixing angle of the CP-violating coupling by $\alpha \leq 43°$ (ATLAS, [15]) and $\alpha \leq 55°$ (CMS, [16]) at 95 % confidence level each.

Current discussions on this topic are mainly done numerically by using simulation software, variations of the Monte Carlo method, or machine learning (see e.g. [12, 17, 18]).

This thesis has the goal of approaching the leading order analysis of the $q\bar{q} \to t\bar{t}H$ process in a mainly analytical way, providing a tangible expression for the resulting amplitudes. The resulting expressions will then be used to conduct additional analysis regarding the influence of CP-violation for the Higgs-top coupling at different mixing angles α, as well as other correlations between physical observables and the external conditions of the experiments. It also allows for further investigations regarding a high energy limit, as well as different helicity initial states. Throughout this thesis, natural units will be used.

All occurring images of Feynman diagrams and plots are made with *FeynGame* [19] and the *matplotlib* library [20] for the *Python* language respectively.
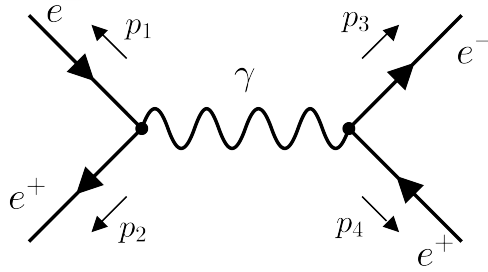
2 Basics

2.1 Feynman diagrams

Figure 1: Example of a Feynman diagram, which shows a possible process for $e^- e^+ \to e^- e^+$

One of the most relevant discussions in particle physics is the understanding of certain interactions between particles. A very useful tool for describing these interactions are Feynman diagrams. Such a diagram visually shows the order and type of interaction.

A Feynman diagram consists of external and internal particles, which are connected via vertices that act as interaction points. The external particles have loose ends, representing the ingoing or outgoing particles. The internal lines are also called the propagators and transfer some form of physical quantity in the form of virtual exchange particles.

An example is shown in figure 1. Time is drawn to the right, while space is pointing upwards. The arrows on the incoming and outgoing lines represent the particle flow. It shows an electron e^- with momentum p_1 and a positron e^+ with momentum p_2, which collide and annihilate into a virtual photon γ. This photon then decays into another electron-positron pair. The momenta are all pointing outwards, which is a convention that will be used on all occasions throughout this thesis.

In general, there are multiple ways of describing the interaction between certain incoming and outgoing particles, each corresponding to a separate Feynman diagram. The main goal of these discussions is to obtain the cross-section of this process, which is a measure of how likely this specific process is at a real measurement. The cross-section heavily depends on the absolute square of the main amplitude for such a process, which is also often called the associated matrix element. If $\mathcal{M}_i$ for $i \in \mathbb{N}$ are the amplitudes for individual sub-processes with the same incoming and outgoing particles, as described by single Feynman diagrams, then the total amplitude is just the sum of the $\mathcal{M}_i$. The absolute square is then given by

$$|\mathcal{M}|^2 = \left(\sum_i \mathcal{M}_i\right)\left(\sum_i \mathcal{M}_i\right)^\dagger = \left(\sum_i \mathcal{M}_i\right)\left(\sum_i \mathcal{M}_i^\dagger\right) . \tag{1}$$

By considering quarks and gluons in this interaction, spin and color must also be included. Since it is usually not known what the exact quantum numbers of the incoming particles are, it is necessary to take the average of all possible initial states.

A difference in outgoing states are technically different processes, however, since every possibility provides a contribution to the total cross-section, they can be added together. With this, the squared amplitude becomes

$$|\overline{\mathcal{M}}|^2 = \frac{1}{\tilde{N}} \sum_{\text{spin, color}} \left(\sum_i \mathcal{M}_i \right) \left(\sum_i \mathcal{M}_i^\dagger \right) ,\qquad(2)$$

where $\tilde{N}$ includes the 4 possible incoming spin combinations for a spin $\frac{1}{2}$ particle and the 9 possible color combinations. Therefore $\tilde{N} = 36$.

Considering the leading order of a process then means applying the Born approximation to the underlying perturbation theory and therefore focusing on the most simple form a given interaction. The inclusion of additional interactions, which lead to the same final state, then increases the precision of the model. These more precise calculations are then typically called next-to-leading order, next-to-next-to-leading order, etc.

By doing this, expression (2) will also include mixed terms consisting of multiple individual amplitudes. This stems from the general concept of quantum mechanics that a system can be in a superposition of multiple states at once. The single amplitudes can therefore be considered certain weights to influence what interaction will happen.

2.1.1 Feynman rules

To obtain the amplitude belonging to a specific Feynman diagram, the Feynman rules can be used. These are expressions, which correspond to certain parts of a diagram and can be multiplicatively combined to form the amplitude. The relevant rules for the process discussed here are listed in table 1. The roman letters (a,b) denote color group indices in the adjoint representation of SU(3), while the in- and outgoing particle indices (i,j) refer to the QCD component of the fundamental representation. The greek letters denote the Lorentz indices.
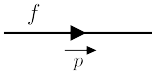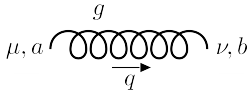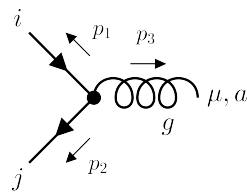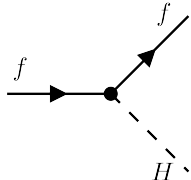
The term $i\varepsilon$ as written in the expressions for the propagators is a general necessity to evade singularities in loop integrations. Since there will be no loop processes in the leading order of quark induced $t\bar{t}H$ production, ε can be set to zero. In addition, for the expression of the gluon propagator, the Feynman gauge can be used, where $\xi_G = 1$, which further simplifies the associated expression. g_s is the strong coupling constant, while g' is the weak isospin coupling. In the fermion-Higgs coupling (table 1), the quantity $v = \frac{2m_W}{g'}$ can be used, where v is the vacuum expectation value and m_W the mass of the W boson.

In addition, the incoming and outgoing fermions are represented by the Dirac spinors and their conjugates

$$\begin{array}{llll}
\text{incoming fermion} & u(p,s) & \text{incoming antifermion} & \overline{v}(p,s) \\
\text{outgoing fermion} & \overline{u}(p,s) & \text{outgoing antifermion} & v(p,s) .
\end{array}$$

p and s are the momentum and the spin of the particle, respectively. The general approach then is to go from left to right in the diagram and follow the particle flow in opposite direction to multiply all factors in the order in which they occur within the diagram. This will result in the amplitude for a specific diagram.

Table 1: A selection of Feynman rules for different elements of a Feynman diagram [21]

Type		Expression
Fermion propagator		$i\dfrac{\not{p}+m_f}{p^2-m_f^2+i\varepsilon}$
Gluon propagator		$-i\delta_{ab}\left[\dfrac{g_{\mu\nu}}{q^2+i\varepsilon} - \left(1-\xi_G\right)\dfrac{q_\mu q_\nu}{(q^2)^2}\right]$
Fermion-gluon vertex		$-ig_s\gamma^\mu T^a_{ij}$
Fermion-Higgs vertex		$-i\dfrac{g'm_f}{2m_W}$

2.2 Dirac algebra

2.2.1 Dirac matrices and spinors

The Dirac matrices, also often called gamma matrices, are a certain set of 4×4 matrices which for instance occur in the Dirac equation and therefore also generally in quantum field theory. The initially defined matrices are $\gamma^0, \gamma^1, \gamma^2$, and γ^3. These can be written as γ^μ for $\mu \in \{0, 1, 2, 3\}$. An additional matrix γ^5 is often defined as $\gamma^5 = i\gamma^0\gamma^1\gamma^2\gamma^3$, which is used in the context of chirality.

The anticommutator of two Dirac matrices is

$$\{\gamma^\mu, \gamma^\nu\} = 2\eta^{\mu\nu}I ~, \tag{3}$$

where $\eta^{\mu\nu}$ is the Minkowski metric with signature $(+, -, -, -)$ and I is the identity matrix. In particular, this means that $\gamma^0\gamma^0 = I$.

The γ^5 matrix also satisfies $\gamma^5\gamma^5 = I$. With the other matrices, the anticommutator results in

$$\{\gamma^\mu, \gamma^5\} = 0 ~. \tag{4}$$

Generally, these matrices satisfy the relation $\left(\gamma^\mu\right)^\dagger = \gamma^0\gamma^\mu\gamma^0$, from which follows that γ^0 and γ^5 are hermitian.

An additional important expression is the Feynman slash notation

$$\slashed{a} = \gamma^\mu a_\mu \; , \tag{5}$$

where a is an arbitrary four-vector.

Dirac spinors are spinors that represent fermions as plane-wave solutions of the Dirac equation. These can be used as stated in section 2.1.1. The conjugate spinor with respect to spinor ψ is defined as $\overline{\psi} = \psi^\dagger \gamma^0$.

The spinors u and v then satisfy the completeness relation, which means that

$$\sum_s u(p,s)\overline{u}(p,s) = \slashed{p} + m \tag{6}$$

$$\sum_s v(p,s)\overline{v}(p,s) = \slashed{p} - m \; , \tag{7}$$

where m is the mass of the particle described by the specific spinor.

2.2.2 Casimir trick

By using the Feynman rules from chapter 2.1.1, the corresponding amplitude to a specific interaction can be derived. These resulting amplitudes will often include the expression

$$\mathcal{M}' = \overline{v}(p_1)\,\Gamma\,u(p_2) \; , \tag{8}$$

where $\Gamma = \gamma^{\mu_1}\gamma^{\mu_2}\cdot...\cdot\gamma^{\mu_n}$ is an arbitrary string of Dirac matrices. With the properties discussed in section 2.2.1 and by defining $\overline{\Gamma} = \gamma^0\,\Gamma^\dagger\gamma^0$, it follows

$$(\mathcal{M}')^\dagger = u^\dagger(p_2)\,\Gamma^\dagger\,\overline{v}^\dagger(p_1) = \overline{u}(p_2)\,\gamma^0\,\Gamma^\dagger\,\gamma^0\,v(p_1) = \overline{u}(p_2)\,\overline{\Gamma}\,v(p_1) \; . \tag{9}$$

Since the square of the amplitude is of interest, a trick can be used to make the expression more manageable. All spinors and matrices in amplitude (8) can be written in the index notation in combination with Einstein notation. If the amplitude is then calculated as in equation (2) and by using the knowledge from section 2.2.1, it will lead to

$$\sum_{\text{spin}} \overline{v}(p_1)\,\Gamma\,u(p_2) \cdot \left[\overline{v}(p_1)\,\Gamma\,u(p_2)\right]^\dagger = \sum_{\text{spin}} \overline{v}_\alpha(p_1)\,\Gamma_{\alpha\beta}\,u_\beta(p_2)\,\overline{u}_{\beta'}(p_2)\,\overline{\Gamma}_{\beta'\alpha'}\,v_{\alpha'}(p_1) \tag{10}$$

$$= \sum_{\text{spin}} \Gamma_{\alpha\beta}\left[u(p_2)\,\overline{u}(p_2)\right]_{\beta\beta'}\overline{\Gamma}_{\beta'\alpha'}\left[v(p_1)\,\overline{v}(p_1)\right]_{\alpha'\alpha}$$

$$= \sum_{\text{spin}} \left[\Gamma\,u(p_2)\,\overline{u}(p_2)\,\overline{\Gamma}\,v(p_1)\,\overline{v}(p_1)\right]_{\alpha\alpha}$$

$$\overset{(6),(7)}{=} \text{Tr}\left[\Gamma\,(\slashed{p}_2 + m_2)\,\overline{\Gamma}\,(\slashed{p}_1 - m_1)\right] \; .$$

With this method, which is known as the Casimir-Trick, the squared expression can be written in terms of traces over gamma matrices and momenta. These can then be evaluated more easily by hand or with the help of computer programs.

3 $t\bar{t}H$ production in the Standard Model

3.1 Amplitude

The goal is to derive the leading order amplitude for the process, which will lead to $t\bar{t}H$ production. While gluon initial states are also able to produce this result, only the quark initial state will be considered in this case. One possibility to create the Higgs boson and a top quark is the process shown in figure 2. Two light quarks annihilate into a gluon, which decays into a top quark / top antiquark pair. One of the created top quarks can then spontaneously emit a Higgs boson.

These two shown interactions are not the only ones that will lead to the wanted result. However, other possibilities in leading order do not rely on the strong force or the coupling between the Higgs boson and the top quark. This will result in amplitudes that are at least an order of magnitude smaller than the ones shown in figure 2 and can therefore be neglected.

By applying the rules discussed in section 2.1.1, the amplitudes for the described processes result in

$$\mathcal{M}_1 = i \frac{g_s^2}{q^2 + i\varepsilon} \frac{m_t}{v} T_{ij}^a T_{lk}^a \left[\overline{v}(-p_2, s_2) \gamma^\mu u(-p_1, s_1) \overline{u}(p_3, s_3) \left(\frac{-\not{p} + m_t}{p^2 - m_t^2 + i\varepsilon} \right) \gamma_\mu v(p_4, s_4) \right] \quad (11)$$

$$\mathcal{M}_2 = i \frac{g_s^2}{q^2 + i\varepsilon} \frac{m_t}{v} T_{ij}^a T_{lk}^a \left[\overline{v}(-p_2, s_2) \gamma^\mu u(-p_1, s_1) \overline{u}(p_3, s_3) \gamma_\mu \left(\frac{\not{p}' + m_t}{p'^2 - m_t^2 + i\varepsilon} \right) v(p_4, s_4) \right] , \quad (12)$$

where $q = -(p_1 + p_2)$ is the momentum of the gluon propagator, $p = p_3 + p_5$ the momentum of the fermion propagator for figure 2 (1) and $p' = p_4 + p_5$ the momentum of the fermion propagator for figure 2 (2). m_t is the top quark mass. Now, following the principle from section 2.1 the squared amplitude becomes

$$\overline{|\mathcal{M}|}^2 = \frac{1}{(nN)^2} \lim_{\varepsilon \to 0} \sum_{\text{spin, color}} (\mathcal{M}_1 + \mathcal{M}_2)(\mathcal{M}_1^\dagger + \mathcal{M}_2^\dagger) , \quad (13)$$

where $n = 2$ and $N = 3$ are the amount of possible spin and color states, respectively, of a single incoming particle in this case. It can also be used that the generators of SU(N) satisfy the condition $T_{ij}^a T_{lk}^a = \frac{1}{2}(\delta_{ik}\delta_{jl} - \frac{1}{N}\delta_{ij}\delta_{lk})$ which will lead to $(T_{ij}^a T_{lk}^a)(T_{ij}^a T_{lk}^a)^\dagger = \frac{1}{2} C_A C_F$, where $C_A = N$ and $C_F = \frac{N^2-1}{2N}$ are the eigenvalues of the Casimir operator. By additionally using the Casimir trick from chapter 2.2.2, equation (13) will produce

$$\overline{|\mathcal{M}|}^2 = \frac{1}{(nN)^2} \frac{g_s^4 m_t^2 C_A C_F}{2q^2 v^2} \text{Tr} \left[\gamma^\mu (-\not{p}_1 + m_1) \gamma^{\mu'} (-\not{p}_2 + m_2) \right] \quad (14)$$

$$\cdot \left\{ \frac{1}{(p^2 - m_t^2)^2} \text{Tr} \left[\gamma_\mu (-\not{p} + m_t)(\not{p}_4 - m_t)(-\not{p} + m_t)\gamma_{\mu'}(\not{p}_3 + m_t) \right] \right.$$

$$+ \frac{1}{(p'^2 - m_t^2)^2} \text{Tr} \left[(\not{p}' + m_t)\gamma_\mu(\not{p}_4 - m_t)\gamma_{\mu'}(\not{p}' + m_t)(\not{p}_3 + m_t) \right]$$

$$+ \frac{1}{(p^2 - m_t^2)(p'^2 - m_t^2)} \text{Tr} \left[\gamma_\mu (-\not{p} + m_t)(\not{p}_4 - m_t)\gamma_{\mu'}(\not{p}' + m_t)(\not{p}_3 + m_t) \right]$$

$$+ \left. \frac{1}{(p^2 - m_t^2)(p'^2 - m_t^2)} \text{Tr} \left[(\not{p}' + m_t)\gamma_\mu(\not{p}_4 - m_t)(-\not{p} + m_t)\gamma_{\mu'}(\not{p}_3 + m_t) \right] \right\} .$$
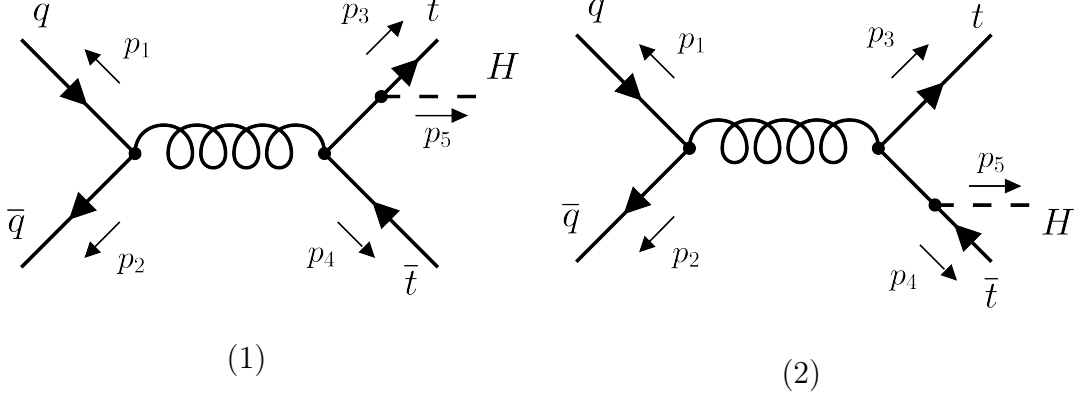
Figure 2: Relevant Feynman diagrams for the process $q\bar{q} \to t\bar{t}H$

To obtain a clear analytical representation of the amplitude, the traces can be calculated explicitly. This is done by using the *Tracer* package [22] for the *Mathematica* software. It can now also be used that the two incoming quarks are light and their masses m_1 and m_2 are therefore negligible in regard to the top quark and Higgs boson mass. The different momenta can then be written as $q^2 = (p_1 + p_2)^2 = 2p_1p_2$, $p^2 = m_t^2 + m_h^2 + 2p_4p_5$ and $p' = m_t^2 + m_h^2 + 2p_3p_5$, where m_h is the Higgs boson mass. After simplification, the squared amplitude becomes

$$
\begin{aligned}
|\overline{\mathcal{M}}|^2 = &\frac{1}{(nN)^2} \cdot \frac{4C_A C_F m_t^2 g_s^4}{v^2 p_{12}^2} \Bigg\{ \frac{2}{(m_h^2 + 2p_{35})(m_h^2 + 2p_{45})} \Big[m_h^2(p_{12}p_{34} - p_{13}p_{24} - p_{14}p_{23}) \\
&+ 2m_t^2\Big(p_{12}(p_{35} + p_{45}) + p_{13}(2p_{24} + p_{25}) + p_{14}(2p_{23} + p_{25}) + p_{15}(p_{23} + p_{24} + p_{25})\Big) \\
&+ 4m_t^4 p_{12} + p_{25}(p_{45}p_{13} + p_{14}p_{35} - p_{15}p_{34}) + p_{15}(p_{23}p_{45} + p_{24}p_{35} - p_{25}p_{34}) \Big] \\
&+ \frac{1}{(m_h^2 + 2p_{35})^2}\Big[m_h^2(m_t^2 p_{12} - p_{13}p_{24} - p_{14}p_{23}) \\
&+ 4m_t^2\Big(p_{12}(p_{35} + m_t^2) + p_{24}(p_{13} + p_{15}) + p_{14}(p_{23} + p_{25})\Big) + 2p_{35}(p_{14}p_{25} + p_{15}p_{24}) \Big] \\
&+ \frac{1}{(m_h^2 + 2p_{45})^2}\Big[m_h^2(m_t^2 p_{12} - p_{13}p_{24} - p_{14}p_{23}) \\
&+ 4m_t^2\Big(p_{12}(p_{45} + m_t^2) + p_{13}(p_{24} + p_{25}) + p_{23}(p_{14} + p_{15})\Big) + 2p_{45}(p_{13}p_{25} + p_{15}p_{23}) \Big] \Bigg\},
\end{aligned}
\tag{15}
$$

where the notation $p_{ij} = p_i p_j$ has been used. From here, an observation can be made. The incoming momenta p_1 and p_2 appear very often in expression (15) in a alternating manner. The combination $p_{1i}p_{2j}$ for instance, where p_i and p_j are arbitrary momenta, occurs together with its symmetrical counterpart $p_{1j}p_{2i}$. Therefore, a symmetrical combination of momenta can be introduced by

$$
\lambda_{ij} = p_{1i}p_{2j} + p_{1j}p_{2i} .
\tag{16}
$$

8

By substituting this into the amplitude, equation (15) gets the more compact form

$$
\begin{aligned}
|\overline{\mathcal{M}}|^2 = \frac{1}{(nN)^2} \cdot \frac{4C_A C_F m_t^2 g_s^4}{v^2 p_{12}^2} & \Bigg\{ \frac{2}{(m_h^2 + 2p_{35})(m_h^2 + 2p_{45})} \Big[m_h^2(p_{12}p_{34} - \lambda_{34}) \\
& + 2m_t^2 \Big(p_{12}(p_{35} + p_{45} + 2m_t^2) + 2\lambda_{34} + \lambda_{45} + \lambda_{35} \Big) + p_{45}\lambda_{35} + p_{35}\lambda_{45} - \lambda_{55}(p_{34} - m_t^2) \Big] \\
& + \frac{1}{(m_h^2 + 2p_{35})^2} \Big[m_h^2(m_t^2 p_{12} - \lambda_{34}) + 4m_t^2 \Big(p_{12}(p_{35} + m_t^2) + \lambda_{34} + \lambda_{45} \Big) + 2p_{35}\lambda_{45} \Big] \\
& + \frac{1}{(m_h^2 + 2p_{45})^2} \Big[m_h^2(m_t^2 p_{12} - \lambda_{34}) + 4m_t^2 \Big(p_{12}(p_{45} + m_t^2) + \lambda_{34} + \lambda_{35} \Big) + 2p_{45}\lambda_{35} \Big] \Bigg\} .
\end{aligned}
\tag{17}
$$

This expression has been verified by numerically comparing it to the result from *FeynCalc* [23–25], an extension for the *Mathematica* software, for the same process. The analytical amplitude for the $q\bar{q} \to t\bar{t}H$ interaction has also been derived before [26], which is also in accordance with expression (15) and (17) by numerical evaluation.

This expression now also clearly shows the symmetry of the system. The λ_{ij} element is obviously invariant in respect to switching the indices i and j and the momenta p_1 and p_2. Thus, it can be seen that the whole equation (17) does not change under the transformation $(3,4) \to (4,3)$ or $(1,2) \to (2,1)$. The last two lines are identical except for the switched indices 3 and 4. What remains only includes symmetrical combinations like $p_{35} + p_{45}$. This is to be expected, as both of the used diagrams from figure 2 as a whole are also symmetrical under these transformations.

By using the *POWHEG BOX* framework [27–29] with a specific implementation for the $t\bar{t}H$ process (by J. Lang, compare with e.g. [30]), the squared amplitude can be converted to the actual cross-section by numerical methods. For 10^5 random events at a center-of-mass energy of $\sqrt{s} = 13\,\text{TeV}$, this results into a value of

$$
\sigma_{q\bar{q} \to t\bar{t}H} = (120.22 \pm 0.11)\,\text{fb} .
\tag{18}
$$

Another important process that is also present at the LHC measurements in the search for the Higgs boson is the gluon initial state, i.e. $gg \to t\bar{t}H$. This is a natural contribution because the LHC uses proton collisions. With the *POWHEG BOX* implementation and the same settings, this returns

$$
\sigma_{gg \to t\bar{t}H} = (629.63 \pm 0.71)\,\text{fb} .
\tag{19}
$$

So the importance of the $q\bar{q} \to t\bar{t}H$ channel becomes clear since the quark initial state is about $19,09\,\%$ of the gluon initial state, where the latter is the main contributor in $t\bar{t}H$ production. Thus, the quark-antiquark interaction can not be neglected in all measurements.

4 $t\bar{t}H$ production with anomalous Higgs-top coupling

4.1 Amplitude

To introduce a CP-violating coupling between the Higgs boson and the top quark, the expression for the corresponding vertex can be adjusted. A possible way of parametrizing the amount of CP-violation (see e.g. [12,17]) is choosing the coupling to be

$$-\frac{m_t}{v}\kappa_t\big(\cos(\alpha) + i\gamma_5\sin(\alpha)\big) \ . \tag{20}$$

Therefore, the Feynman rule for the Fermion-Higgs vertex from Table 1 will now be expression (20). α then represents a sort of phase to tweak the exact coupling effects. The Standard Model is described by choosing $\alpha = 0$ and $\kappa_t = 1$. The amplitudes for the processes represented in figure 2 then become

$$\mathcal{M}_1 = \eta \cdot \left[\bar{v}(-p_2, s_2)\gamma^\mu u(-p_1, s_1)\bar{u}(p_3, s_3)\big(\cos(\alpha) + i\gamma^5\sin(\alpha)\big)\left(\frac{-\slashed{p} + m_t}{p^2 - m_t^2}\right)\gamma_\mu v(p_4, s_4)\right] \tag{21}$$

$$\mathcal{M}_2 = \eta \cdot \left[\bar{v}(-p_2, s_2)\gamma^\mu u(-p_1, s_1)\bar{u}(p_3, s_3)\gamma_\mu\left(\frac{\slashed{p}' + m_t}{p'^2 - m_t^2}\right)\big(\cos(\alpha) + i\gamma^5\sin(\alpha)\big)v(p_4, s_4)\right] \tag{22}$$

$$\text{with } \eta = i\frac{g_s^2 m_t}{q^2 v}\kappa_t T_{ij}^a T_{lk}^a \ ,$$

where, again, $q = -(p_1 + p_2)$, $p = p_3 + p_5$ and $p' = p_4 + p_5$. In the same way as shown in chapter 3, the squared amplitude is given by

$$|\overline{\mathcal{M}}|^2_{\text{CPV}} = \frac{1}{(nN)^2} \cdot \frac{4C_A C_F m_t^2 g_s^4 \kappa_t}{v^2 p_{12}^2}\Bigg\{\frac{2}{(m_h^2 + 2p_{35})(m_h^2 + 2p_{45})} \tag{23}$$

$$\cdot \Big[m_t^2\cos(2\alpha)\Big(p_{12}(2m_t^2 + p_{35} + p_{45}) + 2p_{13}p_{24} + 2p_{14}p_{23} + p_{15}p_{23} + p_{15}p_{24}$$

$$+ p_{25}(p_{13} + p_{14} + 2p_{15})\Big)$$

$$+ m_t^2\Big(p_{12}(p_{35} + p_{45} + 2m_t^2) + p_{13}(2p_{24} + p_{25}) + p_{14}(2p_{23} + p_{25}) + p_{15}(p_{23} + p_{24})\Big)$$

$$- m_h^2(-p_{12}p_{34} + p_{13}p_{24} + p_{14}p_{23}) + p_{13}p_{25}p_{45} + p_{14}p_{25}p_{35} + p_{15}p_{23}p_{45}$$

$$+ p_{15}p_{24}p_{35} - 2p_{15}p_{25}p_{34}\Big]$$

$$+ \frac{1}{(m_h^2 + 2p_{35})^2}\Big[m_t^2\cos(2\alpha)\Big(m_h^2 p_{12} + 2\{p_{12}(m_t^2 + p_{35}) + p_{24}(p_{13} + p_{15}) + p_{14}(p_{23} + p_{25})\}\Big)$$

$$- m_h^2(p_{13}p_{24} + p_{14}p_{23}) + 2m_t^2\Big(p_{12}p_{35} + p_{24}(p_{13} + p_{15}) + p_{14}(p_{23} + p_{25})\Big)$$

$$+ 2m_t^4 p_{12} + 2p_{35}(p_{14}p_{25} + p_{15}p_{24})\Big]$$

$$+ \frac{1}{(m_h^2 + 2p_{45})^2}\Big[m_t^2\cos(2\alpha)\Big(m_h^2 p_{12} + 2\{p_{12}(m_t^2 + p_{45}) + p_{13}(p_{24} + p_{25}) + p_{23}(p_{14} + p_{15})\}\Big)$$

$$- m_h^2(p_{13}p_{24} + p_{14}p_{23}) + 2m_t^2\Big(p_{12}p_{45} + p_{13}(p_{24} + p_{25}) + p_{23}(p_{14} + p_{15})\Big)$$

$$+ 2m_t^4 p_{12} + 2p_{45}(p_{13}p_{25} + p_{15}p_{23})\Big]\Bigg\} \ .$$

By using the substitution (16), expression (23) simplifies to

$$
\begin{aligned}
|\overline{\mathcal{M}}|^2_{\text{CPV}} = {} & \frac{1}{(nN)^2} \cdot \frac{4C_A C_F m_t^2 g_s^4 \kappa_t}{v^2 p_{12}^2} \Bigg\{ \frac{2}{(m_h^2 + 2p_{35})(m_h^2 + 2p_{45})} \Big[- m_h^2(\lambda_{34} - p_{12}p_{34}) \\
& + m_t^2 \big(1 + \cos(2\alpha)\big)\big(p_{12}(p_{35} + p_{45} + 2m_t^2) + 2\lambda_{34} + \lambda_{35} + \lambda_{45} + \lambda_{55}\big) \\
& + \lambda_{35}p_{45} + \lambda_{45}p_{35} - \lambda_{55}(p_{34} + m_t^2) \Big] \\
& + \frac{1}{(m_h^2 + 2p_{35})^2} \Big[m_t^2\big(1 + \cos(2\alpha)\big)\big(m_h^2 p_{12} + 2\{p_{12}(p_{35} + m_t^2) + \lambda_{34} + \lambda_{45}\}\big) \\
& + 2p_{35}\lambda_{45} - m_h^2(\lambda_{34} + p_{12}m_t^2) \Big] \\
& + \frac{1}{(m_h^2 + 2p_{45})^2} \Big[m_t^2\big(1 + \cos(2\alpha)\big)\big(m_h^2 p_{12} + 2\{p_{12}(p_{45} + m_t^2) + \lambda_{34} + \lambda_{35}\}\big) \\
& + 2p_{45}\lambda_{35} - m_h^2(\lambda_{34} + p_{12}m_t^2) \Big] \Bigg\} \,.
\end{aligned}
\tag{24}
$$

This simplified expression for the amplitude has also been verified, similar to section 3, by comparing it to the *FeynCalc* result, where the CP-violating coupling has been inserted manually. In case of the Standard Model ($\alpha = 0$), it can also be noticed that $|\overline{\mathcal{M}}|^2_{\text{CPV}} = |\overline{\mathcal{M}}|^2$, which further confirms the correctness.

The α dependency of the amplitude is only contained in the occurrences of the cos function. Since this only appears in the form $\cos(2\alpha)$, the relevant range for further analysis is $0 \leq \alpha \leq \frac{\pi}{2}$, since additional values outside of this interval would represent redundancies in the evaluation. This is interesting in that expression (20) does not show this behavior. In the same way, as at the end of section 3, the cross-section can be calculated for different α values. This produces the result shown in figure 3.
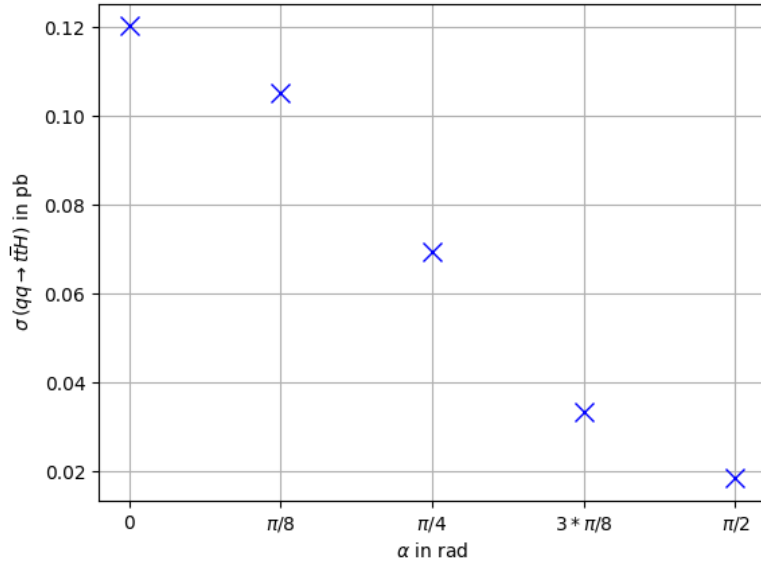

Figure 3: Cross section σ for the $q\bar{q} \to t\bar{t}H$ process for different α values with $\kappa_t = 1$.

4.2 Evaluation for varying α values

Now that the analytical expression for the $q\bar{q} \to t\bar{t}H$ process with CP-violating Higgs-top coupling is available, it can be used to perform additional analysis on the process. By using the partonic center-of-mass energy

$$\beta = \sqrt{1 - \frac{(2m_t + m_H)^2}{(p_1 + p_2)^2}} \ , \tag{25}$$

to characterize the process, where $(p_1 + p_2)^2$ represents the usual center-of-mass energy, the whole range of possible outcomes can be scanned. β will therefore only take the real values $0 \leq \beta < 1$ for physically meaningful scenarios. Furthermore, let $\kappa_t = 1$, since this would otherwise only express itself as a global factor on every result. With this, the expression (24) can be plotted for different values of α in this interval, which produces the graphs in figure 4. Here, an equidistant sampling with 5 values has been used from $\alpha = 0$ to $\alpha = \frac{\pi}{2}$.

By doing this, the influence of α becomes clear. The higher the values of α become, the lower the squared amplitude gets. Since the squared amplitude is a measure of the likelihood of this interaction taking place, it is to be expected that, on average, the total amount of measured events of every physical observable has to decrease for higher α values. Another thing to notice is, that the graphs meet for very high energies. This means, that in a high energy limit, the dependency on α vanishes. This can also be explained analytically, which will be done in section 4.3.

By, again, using the *POWHEG BOX* [27–30] with 10^5 random events at $\sqrt{s} = 13\,\text{TeV}$, other properties of the final products can be determined. A few histograms created from the simulated mass, angle, momentum, rapidity, and pseudorapidity of the outgoing particles can be seen in figure 5 - 9.
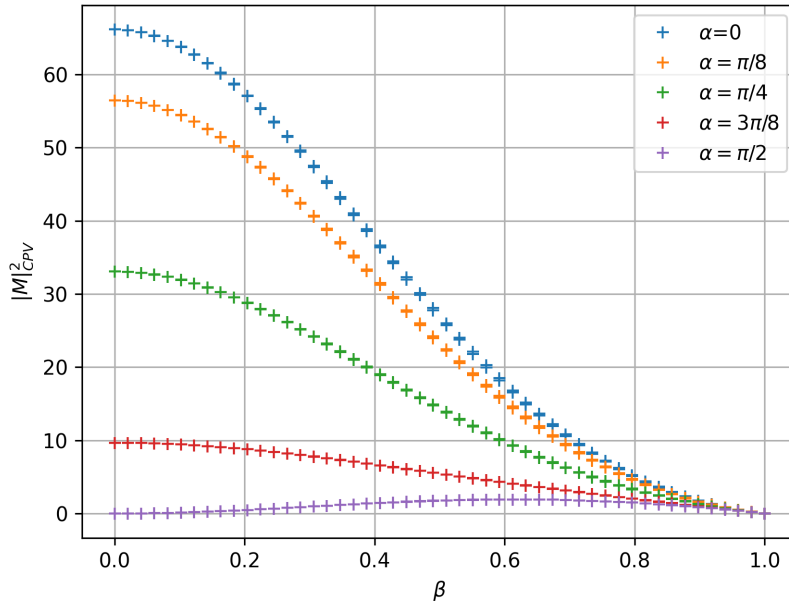

Figure 4: Alpha dependency for the $q\bar{q} \to t\bar{t}H$ amplitude with CP-violating Higgs-top coupling as a function of the partonic center-of-mass energy.
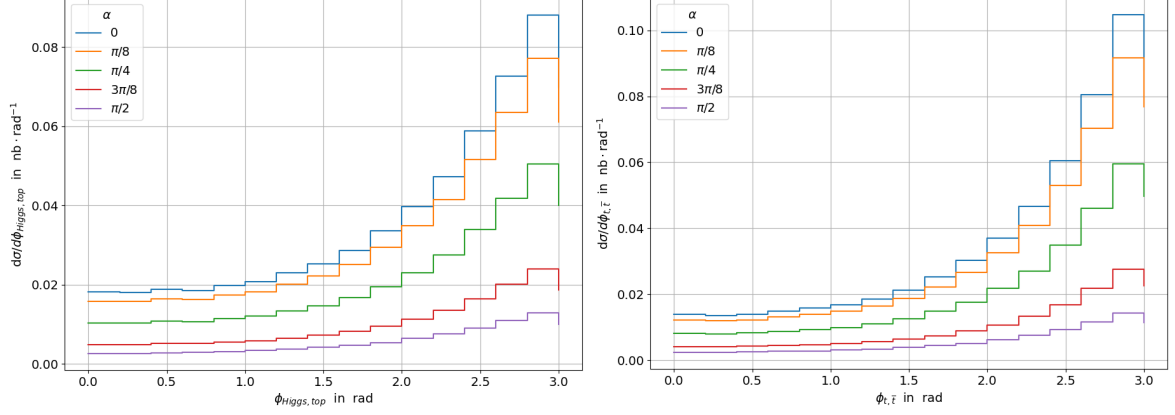
Figure 5: Histograms for the angle $\phi_{\mathrm{H,t}}$ between the Higgs boson and top quark with $(\Delta\phi_{H,t}/\phi_{H,t})_{\mathrm{max}} = 0.55\,\%$, as well as the angle $\phi_{t,\bar{t}}$ between the top quark and the top antiquark with $(\Delta\phi_{t,\bar{t}}/\phi_{t,\bar{t}})_{\mathrm{max}} = 0.50\,\%$ for different α values.
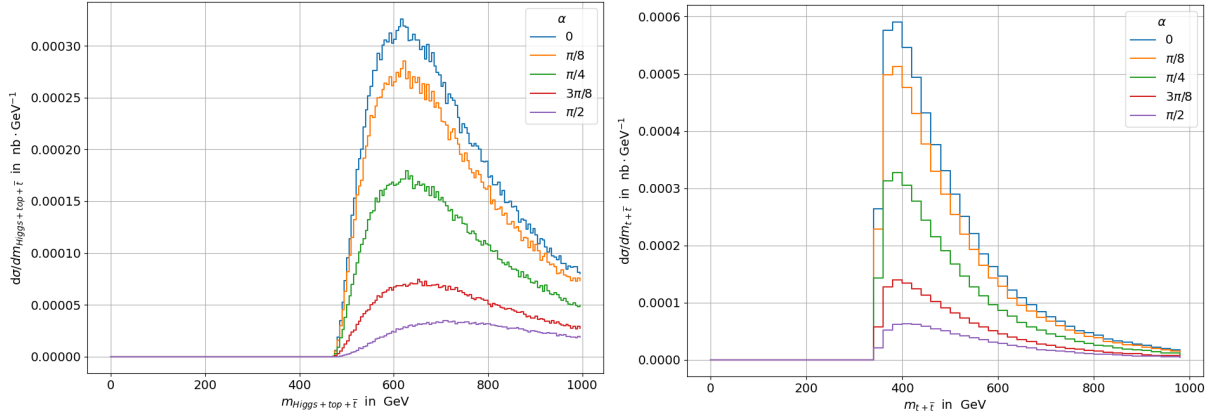

Figure 6: Histograms for the combined mass $m_{H+t+\bar{t}}$ of the Higgs boson, the top quark and top antiquark with $(\Delta m_{H+t+\bar{t}}/m_{H+t+\bar{t}})_{\mathrm{max}} = 1.8\,\%$, as well as the mass $m_{t+\bar{t}}$ of the top quark / top antiquark pair with $(\Delta m_{t+\bar{t}}/m_{t+\bar{t}})_{\mathrm{max}} = 0.70\,\%$ for different α values.

The relative uncertainties resulting from these Monte Carlo integrations do not exceed $(\Delta O/O)_{\mathrm{max}}$ in any bin, as given at every histogram for the observable O.

The effect of varying α clearly stays the same across all observables. For higher values, the amount of relevant events decreases. Characteristic features such as the maximum of each graph remain almost constant, except for $\alpha \approx \frac{\pi}{2}$, where sometimes a slight shift is noticeable (especially in figure 6 and 7). This can also be seen in the graph from the squared amplitude in figure 4, where this initially comes from.

Most of these properties are complementary. The momentum of the Higgs boson, for instance, behaves exactly the same as the $t + \bar{t}$ combination shown in figure 7 on the left. In leading order, this due to the conservation of momentum. Since the process can always be observed in the center-of-mass system, the outgoing momenta must add up to zero, because the initial state only has two particles. Beyond leading order this behavior may deviate, due to QCD radiation.
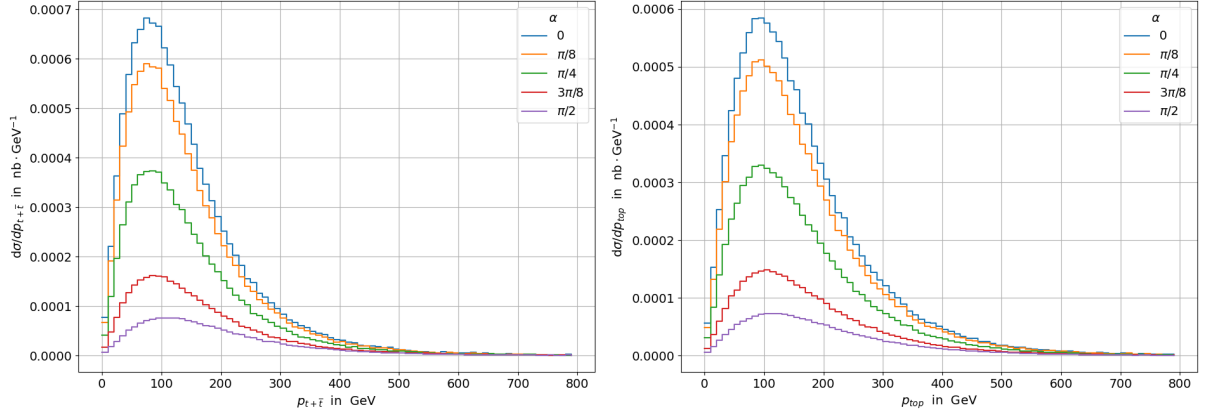
13

Figure 7: Histograms for the momentum p_t of a single top quark with $(\Delta p_t / p_t)_{\max} = 0.99\,\%$, as well as the combined momentum $p_{t+\bar{t}}$ for the top quark / top antiquark pair with $(\Delta p_{t+\bar{t}} / p_{t+\bar{t}})_{\max} = 0.90\,\%$ in transversal direction for different α values.
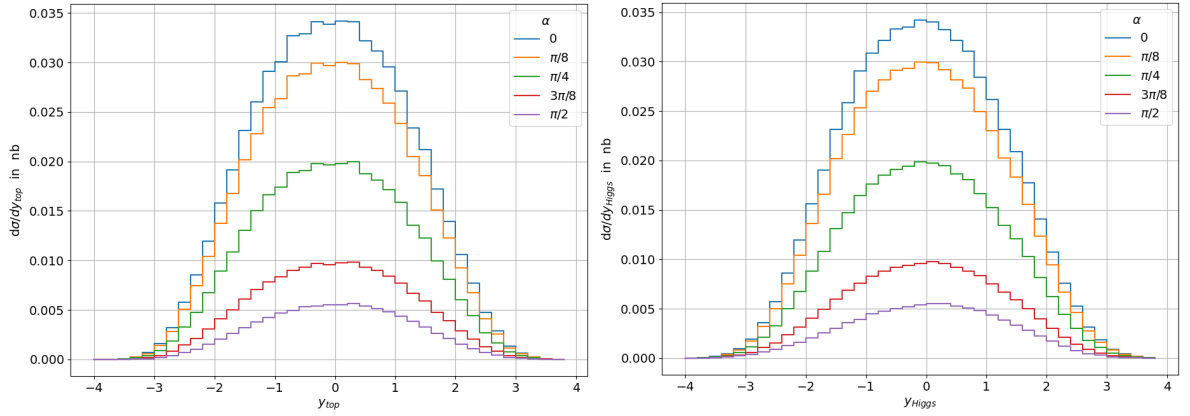

Figure 8: Histograms for the rapidity y_t of the top quark with $(\Delta y_t / y_t)_{\max} = 0.90\,\%$ and y_H for the Higgs boson with $(\Delta y_H / y_H)_{\max} = 0.89\,\%$.
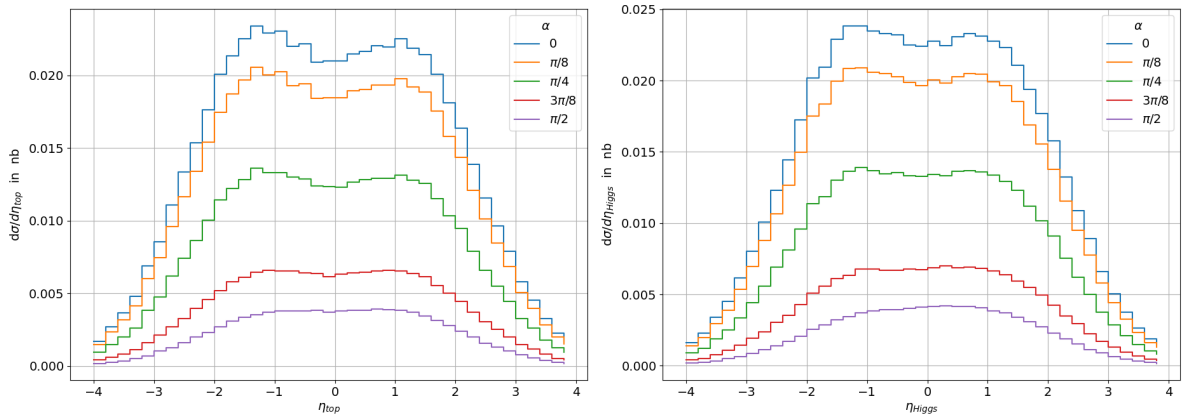
Figure 9: Histograms for the pseudorapidity η_t of the top quark with $(\Delta \eta_t / \eta_t)_{\max} = 1.14\,\%$ and η_H for the Higgs boson with $(\Delta \eta_H / \eta_H)_{\max} = 1.15\,\%$ for different α values.

Rapidity and Pseudorapidity for any particle, as shown in figures 8 and 9, are defined as

$$y = \frac{1}{2} \ln \left(\frac{E + p_l}{E - p_l} \right) \qquad \eta = \operatorname{arctanh} \left(\frac{p_l}{p} \right) ,$$

where E is the energy and p_l the component of the momentum along the beam axis.

4.3 High energy limit

By using Casimir's Trick and the amplitudes from equation (21) and (22), the squared amplitude will be of the form

$$
\begin{aligned}
|\overline{\mathcal{M}}|^2_{\text{CPV}} \propto \text{Tr}\Big[\gamma^\mu \not{p}_1 \gamma^{\mu'} \not{p}_2\Big] \Big(a\Big\{ &\cos^2(\alpha)\text{Tr}\Big[(-\not{p}+m_t)\gamma_\mu(\not{p}_4-m_t)\gamma_{\mu'}(-\not{p}+m_t)(\not{p}_3+m_t)\Big] \quad (26) \\
&+ i\cos(\alpha)\sin(\alpha)\text{Tr}\Big[(-\not{p}+m_t)\gamma_\mu(\not{p}_4-m_t)\gamma_{\mu'}(-\not{p}+m_t)\gamma_5(\not{p}_3+m_t)\Big] \\
&+ i\cos(\alpha)\sin(\alpha)\text{Tr}\Big[\gamma_5(-\not{p}+m_t)\gamma_\mu(\not{p}_4-m_t)\gamma_{\mu'}(-\not{p}+m_t)(\not{p}_3+m_t)\Big] \\
&- \sin^2(\alpha)\text{Tr}\Big[\gamma_5(-\not{p}+m_t)\gamma_\mu(\not{p}_4-m_t)\gamma_{\mu'}(-\not{p}+m_t)\gamma_5(\not{p}_3+m_t)\Big]\Big\} \\
&+ b\Big\{ \cos^2(\alpha)\cdots + i\cos(\alpha)\sin(\alpha)\cdots + \sin^2(\alpha)\ldots\Big\} + c\ldots\Big) ,
\end{aligned}
$$

where a, b and c are coefficients without further relevance in this discussion. Because the simplified term of this expression is already known as equation (23) or (24), it can be seen that the final result only depends on α as the argument of cos functions. Therefore, the squared amplitude is invariant under a change of the sign of α. The expression from equation (26) must obviously also show this behavior, which is why all terms including an odd number of sin functions can be removed. This can also be seen by writing the same expression again but with the substitution $\alpha \to -\alpha$. Since the squared amplitude does not change under this transformation, all terms which receive a minus sign have to be zero because they would otherwise change the result. By doing this, equation (26) becomes

$$
\begin{aligned}
|\overline{\mathcal{M}}|^2_{\text{CPV}} \propto \text{Tr}\Big[\gamma^\mu \not{p}_1 \gamma^{\mu'} \not{p}_2\Big] \Big(a\Big\{ &\cos^2(\alpha)\text{Tr}\Big[(-\not{p}+m_t)\gamma_\mu(\not{p}_4-m_t)\gamma_{\mu'}(-\not{p}+m_t)(\not{p}_3+m_t)\Big] \quad (27) \\
&- \sin^2(\alpha)\text{Tr}\Big[\gamma_5(-\not{p}+m_t)\gamma_\mu(\not{p}_4-m_t)\gamma_{\mu'}(-\not{p}+m_t)\gamma_5(\not{p}_3+m_t)\Big]\Big\} \\
&+ b\Big\{ \cos^2(\alpha)\cdots + \sin^2(\alpha)\ldots\Big\} + c\ldots\Big) .
\end{aligned}
$$

Now, if the limit $s = (p_1+p_2)^2 \to \infty$ is used, the mass m_t becomes negligible in regards to at least two Lorentz invariants formed by p_3, p_4 or p_5. By using the commutator relations for the gamma matrices and the invariance of the trace under cyclic permutations, the trace expression from the second line of equation (27) will result in

$$
\begin{aligned}
\lim_{s\to\infty} &\text{Tr}\Big[\gamma_5(-\not{p}+m_t)\gamma_\mu(\not{p}_4-m_t)\gamma_{\mu'}(-\not{p}+m_t)\gamma_5(\not{p}_3+m_t)\Big] \quad (28) \\
&= \text{Tr}\Big[\gamma_5\not{p}\gamma_\mu\not{p}_4\gamma_{\mu'}\not{p}\gamma_5\not{p}_3\Big] = -\text{Tr}\Big[\not{p}\gamma_\mu\not{p}_4\gamma_{\mu'}\not{p}\not{p}_3\Big] ,
\end{aligned}
$$

which is the same trace expression as in the first line of equation (27). In this case, it was assumed that m_t is negligible in regards to all momenta. However, even if this is not the case, this argument stays valid, since the expression is always in such a way that the commutator relations can be used where this approximation is applicable.

This can be done for every trace expression from equation (27). The trigonometric functions can then be combined by using $\cos^2(\alpha) + \sin^2(\alpha) = 1$, giving

$$\lim_{s \to \infty} |\overline{\mathcal{M}}|^2_{\text{CPV}} \propto \text{Tr}\left[\gamma^\mu \slashed{p}_1 \gamma^{\mu'} \slashed{p}_2\right] \left(a \, \text{Tr}\left[(-\slashed{p} + m_t)\gamma_\mu(\slashed{p}_4 - m_t)\gamma_{\mu'}(-\slashed{p} + m_t)(\slashed{p}_3 + m_t)\right]\right. \tag{29}$$
$$\left. + b \ldots + c \ldots\right),$$

which no longer has any dependency on α. This explains the result for high energies found in figure 4.

4.4 Spinor-helicity formalism

To further specify the initial state of the $q\bar{q} \to t\bar{t}H$ process, a formalism can be used to distinguish the initial and final helicities for both the incoming and outgoing quarks respectively (see e.g. [31]). For that, a spinor can be written in an expanded form

$$u^\pm(p, m) = |\tilde{p}\pm\rangle + \frac{m}{\langle\tilde{p}^\pm|q^\mp\rangle}|q^\mp\rangle$$
$$\overline{u}^\pm(p, m) = \langle\tilde{p}^\pm| + \frac{m}{\langle q^\mp|\tilde{p}^\pm\rangle}\langle q^\mp|$$
$$v^\mp(p, m) = |\tilde{p}\pm\rangle - \frac{m}{\langle\tilde{p}^\pm|q^\mp\rangle}|q^\mp\rangle$$
$$\overline{v}^\mp(p, m) = \langle\tilde{p}^\pm| - \frac{m}{\langle q^\mp|\tilde{p}^\pm\rangle}\langle q^\mp|,$$

where $\lim_{m \to 0} p = \tilde{p}$ and $\tilde{p} = p - \frac{p^2}{2pq}q$. The notation is $|p^\pm\rangle = u^\pm(p) = v^\mp(p)$ and $\langle p^\pm| = \overline{u}^\pm(p) = \overline{v}^\mp(p)$. The left or right-handed component of a spinor can generally be received by using the corresponding projection operator

$$u^\pm(p) = \Pi^\pm u(p)$$
$$\overline{u}^\pm(p) = \overline{u}(p)\Pi^\mp$$
$$v^\mp(p) = \Pi^\pm v(p)$$
$$\overline{v}^\mp(p) = \overline{v}(p)\Pi^\mp,$$

with $\Pi^\pm = \frac{1 \pm \gamma^5}{2}$.

If this is used, bra-ket like structures appear in the typical $\langle p^\lambda|\Gamma|q^{\lambda'}\rangle$ form, where Γ is once again an arbitrary combination of Dirac matrices and $\lambda = \pm$ denotes an arbitrary helicity component. This can be converted to a trace expression by multiplying it with a suitable neutral factor. By doing this, a transformation similar to the Casimir trick can be applied.

This will produce

$$\langle p_i^\lambda | \Gamma | p_i^\lambda \rangle = \text{Tr}\left[\Pi^\lambda \slashed{p}_i \Gamma \right]$$

$$\langle p_i^\lambda | \Gamma | p_j^{-\lambda} \rangle = \frac{\text{Tr}\left[\Pi^{-\lambda} \slashed{p}_j \slashed{p}_i \Gamma \right]}{\langle p_j^{-\lambda} || p_i^\lambda \rangle}$$

$$\langle p_i^\lambda | \Gamma | p_j^\lambda \rangle = \frac{\text{Tr}\left[\Pi^\lambda \slashed{p}_j \slashed{n} \slashed{p}_i \Gamma \right]}{\langle p_j^\lambda | n | p_i^\lambda \rangle}$$

$$\langle p_i^\lambda | \Gamma | p_i^{-\lambda} \rangle = \frac{\text{Tr}\left[\Pi^{-\lambda} \slashed{p}_i \slashed{n}_1 \slashed{n}_2 \slashed{p}_i \Gamma \right]}{\langle p_i^{-\lambda} | n_1 n_2 | p_i^\lambda \rangle} \ ,$$

where the n_i are arbitrary light-like vectors. With this, the primary amplitudes from the $q\bar{q} \to t\bar{t}H$ process can be written in terms of these helicity states. For that, the following can be defined

$$\mathcal{M}_{i1}^{\pm\pm} = \overline{v}_\pm(-p_2) \gamma^\mu u_\pm(-p_1) \tag{30}$$

$$\mathcal{M}_{i1}^{\pm\mp} = \overline{v}_\pm(-p_2) \gamma^\mu u_\mp(-p_1) \ , \tag{31}$$

and

$$\mathcal{M}_{i2,\pm\pm} = \overline{u}_\pm(p_3) \Gamma_{i2} v_\pm(p_4) \tag{32}$$

$$\mathcal{M}_{i2,\pm\mp} = \overline{u}_\pm(p_3) \Gamma_{i2} v_\mp(p_4) \ , \tag{33}$$

so that $\mathcal{M}_{i,\lambda_3\lambda_4}^{\lambda_1\lambda_2} = \eta_i' \cdot \mathcal{M}_{i1}^{\lambda_1\lambda_2} \cdot \mathcal{M}_{i2,\lambda_3\lambda_4}$, for $i = 1, 2$, is the wanted amplitude for one of the two relevant Feynman diagrams from figure 2. Γ_{i1}, Γ_{i2} and η_i then have to be chosen based on the wanted scenario (Standard Model or CPV version). $\lambda_{1/2}$ represents the components for the incoming quarks, while $\lambda_{3/4}$ represents the outgoing quarks. With this structure and all equations from above, these amplitudes can be written in the discussed helicity form. This will result in

$$\mathcal{M}_{i1}^{\pm\pm} = \langle -p_2^\mp | \gamma^\mu | - p_1^\pm \rangle = \frac{\text{Tr}\left[\Pi^\pm \slashed{p}_1 \slashed{p}_2 \gamma^\mu \right]}{\langle -p_1^\pm | - p_2^\mp \rangle} = 0 \tag{34}$$

$$\mathcal{M}_{i1}^{\pm\mp} = \langle -p_2^\mp | \gamma^\mu | - p_1^\mp \rangle = \frac{\text{Tr}\left[\Pi^\mp \slashed{p}_1 \slashed{n} \slashed{p}_2 \gamma^\mu \right]}{\langle -p_1^\mp | n | - p_2^\mp \rangle} \ . \tag{35}$$

Here, $\tilde{p} = p$ can be used since the masses of the incoming quarks are negligible. Expression (34) is equal to zero due to the fact that a trace with an odd number of Dirac matrices, excluding γ^5, is always zero. This means that the helicity components of the initial quarks must be opposite to each other in order to have an interaction.

Furthermore

$$\mathcal{M}_{i2}^{\pm\pm} = \langle \tilde{p}_3^\pm | \Gamma_{i2} | \tilde{p}_4^\mp \rangle + \frac{m_t}{\langle q_3^\mp | \tilde{p}_3^\pm \rangle} \langle q^\mp | \Gamma_{i2} | \tilde{p}_4^\mp \rangle - \frac{m_t}{\langle \tilde{q}_4^\mp | q_4^\pm \rangle} \langle \tilde{p}_3^\pm | \Gamma_{i2} | q_4^\pm \rangle - \frac{m_t^2 \langle q_3^\mp | \Gamma_{i2} | q_4^\pm \rangle}{\langle q_3^\mp | \tilde{p}_3^\pm \rangle \langle \tilde{q}_4^\mp | q_4^\pm \rangle} \quad (36)$$

$$= \frac{\mathrm{Tr}\left[\Pi^\mp \not{\tilde{p}}_4 \not{\tilde{p}}_3 \Gamma_{i2} \right]}{\langle \tilde{p}_4^\mp | \tilde{p}_3^\pm \rangle} + \frac{m_t \mathrm{Tr}\left[\Pi^\mp \not{\tilde{p}}_4 \not{n} \not{q}_3 \Gamma_{i2} \right]}{\langle q_3^\mp | \tilde{p}_3^\pm \rangle \langle \tilde{p}_4^\mp | n | q_3^\mp \rangle} - \frac{m_t \mathrm{Tr}\left[\Pi^\pm \not{q}_4 \not{n} \not{\tilde{p}}_3 \Gamma_{i2} \right]}{\langle \tilde{p}_4^\mp | q_4^\pm \rangle \langle q_4^\pm | n | \tilde{p}_3^\mp \rangle}$$

$$- \frac{m_t^2 \mathrm{Tr}\left[\Pi^\pm \not{q}_4 \not{q}_3 \Gamma_{i2} \right]}{\langle \tilde{p}_4^\mp | q_4^\pm \rangle \langle q_3^\mp | \tilde{p}_3^\pm \rangle \langle q_4^\pm | q_3^\mp \rangle}$$

and in a similar way

$$\mathcal{M}_{i2,\pm\mp} = \frac{\mathrm{Tr}\left[\Pi^\pm \not{\tilde{p}}_4 \not{n} \not{\tilde{p}}_3 \Gamma_{i2} \right]}{\langle \tilde{p}_4^\pm | n | \tilde{p}_3^\pm \rangle} + \frac{m_t \mathrm{Tr}\left[\Pi^\pm \not{\tilde{p}}_4 \not{q}_3 \Gamma_{i2} \right]}{\langle q_3^\mp | \tilde{p}_3^\pm \rangle \langle \tilde{p}_4^\pm | q_3^\mp \rangle} - \frac{m_t \mathrm{Tr}\left[\Pi^\mp \not{q}_4 \not{\tilde{p}}_3 \Gamma_{i2} \right]}{\langle \tilde{p}_4^\pm | q_4^\mp \rangle \langle q_4^\mp | \tilde{p}_3^\pm \rangle} \quad (37)$$

$$+ \frac{m_t^2 \mathrm{Tr}\left[\Pi^\mp \not{q}_4 \not{n} \not{q}_3 \Gamma_{i2} \right]}{\langle \tilde{p}_4^\pm | q_4^\mp \rangle \langle q_3^\mp | \tilde{p}_3^\pm \rangle \langle q_4^\mp | n | q_3^\mp \rangle} \ .$$

So, the final amplitudes in the helicity formalism are

$$\mathcal{M}_{i,\lambda_3\lambda_4}^{\pm\mp} = \eta_i' \cdot \mathcal{M}_{i1}^{\pm\mp} \cdot \mathcal{M}_{i2,\lambda_3\lambda_4} \ , \qquad i = 1,2 \quad (38)$$

where the amplitude vanishes for the $\pm\pm$ combination of incoming quarks, as stated above. In the case of the Standard Model, the gammas and prefactors are

$$\Gamma_{12} = \left[-(\not{p}_3 + \not{p}_5) + m_t \mathbf{1} \right] \gamma_\mu$$

$$\Gamma_{22} = \gamma_\mu \left[(\not{p}_4 + \not{p}_5) + m_t \mathbf{1} \right]$$

$$\eta_1' = i \frac{g_s^2 m_t T_{ij}^a T_{lk}^a}{-(p_1 + p_2)(m_h^2 + 2p_{35})v}$$

$$\eta_2' = i \frac{g_s^2 m_t T_{ij}^a T_{lk}^a}{-(p_1 + p_2)(m_h^2 + 2p_{45})v} \ ,$$

with the identity matrix $\mathbf{1}$. For the CP-violating coupling, they are

$$\Gamma_{12} = \left(\cos(\alpha)\mathbf{1} + i\gamma^5 \sin(\alpha) \right) \left[-(\not{p}_3 + \not{p}_5) + m_t \mathbf{1} \right] \gamma_\mu$$

$$\Gamma_{22} = \gamma_\mu \left[(\not{p}_4 + \not{p}_5) + m_t \mathbf{1} \right] \left(\cos(\alpha)\mathbf{1} + i\gamma^5 \sin(\alpha) \right)$$

$$\eta_1' = i \frac{g_s^2 m_t \kappa_t T_{ij}^a T_{lk}^a}{-(p_1 + p_2)(m_h^2 + 2p_{35})v}$$

$$\eta_2' = i \frac{g_s^2 m_t \kappa_t T_{ij}^a T_{lk}^a}{-(p_1 + p_2)(m_h^2 + 2p_{45})v} \ .$$

This may therefore reveal additional information about the structure of the coupling for the CP-violating scenario by distinguishing the different helicity states, since these expressions may behave differently under variation of α than the usual squared amplitude.

5　Conclusion

To summarize, the search for CP-violating couplings between the Higgs boson and top quark may play a key role in the search for yet unexplained phenomena, like the baryon asymmetry. The quark induced $t\bar{t}H$ channel is, among others, a good candidate for this research, as it is not negligible in regards to the dominant gluon fusion processes at the LHC in the Standard Model (section 3).

To understand this process on a more fundamental level, it can be analyzed from a theoretical point of view. For that, this thesis assumes the usual parametrization of such a coupling (expression (20)) and derives the resulting analytical squared amplitude as equation (24) for the anomalous $q\bar{q} \to t\bar{t}H$ process. While doing this, a combination of kinematic invariants λ_{ij} can be introduced as equation (16) that uses the symmetry of the system to further simplify the expression.

Section 4.2 then analyses the behavior of the squared amplitude under varying values of the CP-violation mixing angle α. This shows that $|\overline{\mathcal{M}}|^2$, and therefore also the cross-section, generally decreases for higher α values. In addition, the dependency on α gradually vanishes at high center-of-mass energies for the initial quarks. This can be explained theoretically by neglecting the top quark mass, as shown in section 4.3. For a further in-depth study of this process, the amplitudes are also presented in terms of the Spinor-helicity formalism in section 4.4. This allows for a more detailed study of the anomalous coupling, due to the possibility of using more precise measurements with regard to helicity.

References

[1] A. D. Sakharov, "Violation of CP Invariance, C asymmetry, and baryon asymmetry of the universe" *Pisma Zh. Eksp. Teor. Fiz.* **5** (1967) 32–35.

[2] F. Englert and R. Brout, "Broken symmetry and the mass of gauge vector mesons" *Phys. Rev. Lett.* **13** (Aug, 1964) 321–323.
https://link.aps.org/doi/10.1103/PhysRevLett.13.321.

[3] P. Higgs, "Broken symmetries, massless particles and gauge fields" *Physics Letters* **12** no. 2, (1964) 132–133.
https://www.sciencedirect.com/science/article/pii/0031916364911369.

[4] P. W. Higgs, "Broken symmetries and the masses of gauge bosons" *Phys. Rev. Lett.* **13** (Oct, 1964) 508–509.
https://link.aps.org/doi/10.1103/PhysRevLett.13.508.

[5] G. S. Guralnik, C. R. Hagen, and T. W. B. Kibble, "Global conservation laws and massless particles" *Phys. Rev. Lett.* **13** (Nov, 1964) 585–587.
https://link.aps.org/doi/10.1103/PhysRevLett.13.585.

[6] P. W. Higgs, "Spontaneous symmetry breakdown without massless bosons" *Phys. Rev.* **145** (May, 1966) 1156–1163.
https://link.aps.org/doi/10.1103/PhysRev.145.1156.

[7] T. W. B. Kibble, "Symmetry breaking in non-abelian gauge theories" *Phys. Rev.* **155** (Mar, 1967) 1554–1561.
https://link.aps.org/doi/10.1103/PhysRev.155.1554.

[8] **ATLAS** Collaboration, G. Aad *et al.*, "Observation of a new particle in the search for the Standard Model Higgs boson with the ATLAS detector at the LHC" *Phys. Lett. B* **716** (2012) 1–29, arXiv:1207.7214 [hep-ex].

[9] **CMS** Collaboration, S. Chatrchyan *et al.*, "Observation of a New Boson at a Mass of 125 GeV with the CMS Experiment at the LHC" *Phys. Lett. B* **716** (2012) 30–61, arXiv:1207.7235 [hep-ex].

[10] **ATLAS** Collaboration, G. Aad *et al.*, "Study of the spin and parity of the Higgs boson in diboson decays with the ATLAS detector" *Eur. Phys. J. C* **75** no. 10, (2015) 476, arXiv:1506.05669 [hep-ex]. [Erratum: Eur.Phys.J.C 76, 152 (2016)].

[11] **CMS** Collaboration, V. Khachatryan *et al.*, "Constraints on the spin-parity and anomalous HVV couplings of the Higgs boson in proton collisions at 7 and 8 TeV" *Phys. Rev. D* **92** no. 1, (2015) 012004, arXiv:1411.3441 [hep-ex].

[12] M. R. Buckley and D. Goncalves, "Boosting the Direct CP Measurement of the Higgs-Top Coupling" *Phys. Rev. Lett.* **116** no. 9, (2016) 091801, arXiv:1507.07926 [hep-ph].

[13] **CMS** Collaboration, A. M. Sirunyan *et al.*, "Observation of t$\bar{\text{t}}$H production" *Phys. Rev. Lett.* **120** no. 23, (2018) 231801, arXiv:1804.02610 [hep-ex].

[14] **ATLAS** Collaboration, M. Aaboud *et al.*, "Observation of Higgs boson production in association with a top quark pair at the LHC with the ATLAS detector" *Phys. Lett. B* **784** (2018) 173–191, `arXiv:1806.00425 [hep-ex]`.

[15] **ATLAS** Collaboration, G. Aad *et al.*, "CP Properties of Higgs Boson Interactions with Top Quarks in the $t\bar{t}H$ and tH Processes Using $H \to \gamma\gamma$ with the ATLAS Detector" *Phys. Rev. Lett.* **125** no. 6, (2020) 061802, `arXiv:2004.04545 [hep-ex]`.

[16] **CMS** Collaboration, A. M. Sirunyan *et al.*, "Measurements of $t\bar{t}H$ Production and the CP Structure of the Yukawa Interaction between the Higgs Boson and Top Quark in the Diphoton Decay Channel" *Phys. Rev. Lett.* **125** no. 6, (2020) 061801, `arXiv:2003.10866 [hep-ex]`.

[17] D. Azevedo, A. Onofre, F. Filthaut, and R. Gonçalo, "CP tests of Higgs couplings in $t\bar{t}h$ semileptonic events at the LHC" *Phys. Rev. D* **98** no. 3, (2018) 033004, `arXiv:1711.05292 [hep-ph]`.

[18] R. K. Barman, D. Gonçalves, and F. Kling, "Machine learning the Higgs boson-top quark CP phase" *Phys. Rev. D* **105** no. 3, (2022) 035023, `arXiv:2110.07635 [hep-ph]`.

[19] R. V. Harlander, S. Y. Klein, and M. Lipp, "FeynGame" *Comput. Phys. Commun.* **256** (2020) 107465, `arXiv:2003.00896 [physics.ed-ph]`.

[20] J. D. Hunter, "Matplotlib: A 2d graphics environment" *Computing in Science & Engineering* **9** no. 3, (2007) 90–95.

[21] J. C. Romao and J. P. Silva, "A resource for signs and Feynman diagrams of the Standard Model" *Int. J. Mod. Phys. A* **27** (2012) 1230025, `arXiv:1209.6213 [hep-ph]`.

[22] M. Jamin and M. E. Lautenbacher, "Tracer version 1.1: A mathematica package for γ-algebra in arbitrary dimensions" *Computer Physics Communications* **74** no. 2, (1993) 265–288. `https://www.sciencedirect.com/science/article/pii/001046559390097V`.

[23] V. Shtabovenko, R. Mertig, and F. Orellana, "FeynCalc 9.3: New features and improvements" *Comput. Phys. Commun.* **256** (2020) 107478, `arXiv:2001.04407 [hep-ph]`.

[24] V. Shtabovenko, R. Mertig, and F. Orellana, "New Developments in FeynCalc 9.0" *Comput. Phys. Commun.* **207** (2016) 432–444, `arXiv:1601.01167 [hep-ph]`.

[25] R. Mertig, M. Bohm, and A. Denner, "FEYN CALC: Computer algebraic calculation of Feynman amplitudes" *Comput. Phys. Commun.* **64** (1991) 345–359.

[26] J. N. Ng and P. Zakarauskas, "A QCD Parton Calculation of Conjoined Production of Higgs Bosons and Heavy Flavors in $p\bar{p}$ Collision" *Phys. Rev. D* **29** (1984) 876.

[27] P. Nason, "A New method for combining NLO QCD with shower Monte Carlo algorithms" *JHEP* **11** (2004) 040, `arXiv:hep-ph/0409146`.

[28] S. Frixione, P. Nason, and C. Oleari, "Matching NLO QCD computations with Parton Shower simulations: the POWHEG method" *JHEP* **11** (2007) 070, `arXiv:0709.2092 [hep-ph]`.

[29] S. Alioli, P. Nason, C. Oleari, and E. Re, "A general framework for implementing NLO calculations in shower Monte Carlo programs: the POWHEG BOX" *JHEP* **06** (2010) 043, `arXiv:1002.2581 [hep-ph]`.

[30] G. Heinrich, J. Lang, and L. Scyboz, "SMEFT predictions for $gg \to hh$ at full NLO QCD and truncation uncertainties" `arXiv:2204.13045 [hep-ph]`.

[31] D. Maitre and P. Mastrolia, "S@M, a Mathematica Implementation of the Spinor-Helicity Formalism" *Comput. Phys. Commun.* **179** (2008) 501–574, `arXiv:0710.5559 [hep-ph]`.